RadioGraphics

CT and MR Imaging of Ovarian Tumors with Emphasis on Differential Diagnosis[1]

Seung Eun Jung, MD • Jae Mun Lee, MD • Sung Eun Rha, MD
Jae Young Byun, MD • Jung Im Jung, MD • Seong Tai Hahn, MD

CME FEATURE

See accompanying test at http://www.rsna.org/education/rg_cme.html

LEARNING OBJECTIVES FOR TEST 1

After reading this article and taking the test, the reader will be able to:

- Describe typical and atypical CT and MR imaging findings in ovarian tumors.
- Identify the specific imaging features of various ovarian tumors.
- Discuss the key features that are helpful in developing a differential diagnosis for these tumors.

Ovarian tumors are classified on the basis of tumor origin as epithelial tumors (serous and mucinous tumors, endometrioid and clear cell carcinomas, Brenner tumor), germ cell tumors (mature and immature teratomas, dysgerminoma, endodermal sinus tumor, embryonal carcinoma), sex cord–stromal tumors (fibrothecoma; granulosa cell, sclerosing stromal, and Sertoli-Leydig cell tumors), and metastatic tumors. Epithelial tumors are primarily cystic and, when malignant, are associated with varying proportions of a solid component. Papillary projections are a distinctive feature of epithelial tumors. Profuse papillary projections are highly suggestive of borderline (low-malignant-potential) or malignant tumor. Ovarian teratomas demonstrate lipid material at computed tomography and magnetic resonance (MR) imaging. Malignant germ cell tumors manifest as a large, complex abdominal mass that contains both solid and cystic components. Tumor markers are helpful in diagnosis. The radiologic appearance of sex cord–stromal tumors varies from small solid masses to large multicystic masses. Granulosa cell tumors are usually large multicystic masses with solid components. Fibrothecoma, sclerosing stromal tumor, and Sertoli-Leydig cell tumors are usually solid masses. Fibromas have very low signal intensity on T2-weighted MR images. Certain radiologic findings predominate for each type of tumor. Knowledge of these key features of ovarian tumors provides the criteria for making a specific diagnosis or substantially narrowing the differential diagnosis.

Abbreviations: FLASH = fast low-angle shot, HCG = human chorionic gonadotropin

Index terms: Ovary, CT, 852.1211 • Ovary, MR, 852.1214 • Ovary, neoplasms, 852.31, 852.32, 852.33

RadioGraphics 2002; 22:1305–1325 • **Published online** 10.1148/rg.226025033

[1]From the Department of Radiology, St Mary's Hospital, Catholic University of Korea, 62 Yeouido-dong, Youngdungpo-gu, Seoul 150-713, Korea (S.E.J., J.M.L., J.I.J., S.T.H.); and the Department of Radiology, Kangnam St Mary's Hospital, Catholic University of Korea, Seoul (S.E.R., J.Y.B.). Recipient of a Certificate of Merit award for an education exhibit at the 2001 RSNA scientific assembly. Received February 20, 2002; revision requested March 19 and received May 8; accepted May 9. **Address correspondence to** J.M.L. (e-mail: *sejung@catholic.ac.kr*).

Introduction

Ovarian tumors are classified as epithelial tumors, germ cell tumors, sex cord–stromal cell tumors, and metastatic tumors on the basis of tumor origin (Table 1) (1). Although ovarian tumors have similar clinical and radiologic features, predominant or specific imaging features may be present in some types of ovarian tumors. Characterization of an ovarian mass is of the utmost importance in the preoperative evaluation of an ovarian neoplasm. It enables the surgeon to anticipate carcinoma of the ovary before the operation so that adequate procedures can be planned (2). In recent years, surgical laparoscopy has been used to manage benign adnexal masses with minimal surgical morbidity (3). Therefore, familiarity with the clinical and imaging features of various ovarian tumors is important in determining the likelihood of a tumor being benign or malignant. In this article, we review the imaging, pathologic, and clinical features of ovarian tumors with emphasis on the computed tomographic (CT) and magnetic resonance (MR) imaging features that indicate a specific diagnosis or allow substantial narrowing of the differential diagnosis.

Table 1
Classification of Ovarian Tumors

- Epithelial tumors
  - Serous
  - Mucinous
  - Endometrioid
  - Clear cell
  - Brenner
  - Undifferentiated
- Germ cell tumors
  - Teratoma
    - Mature
    - Immature
  - Dysgerminoma
  - Endodermal sinus tumor
  - Embryonal cell carcinoma
  - Choriocarcinoma
- Sex cord–stromal tumors
  - Granulosa-stromal cell tumors
    - Granulosa cell tumor
    - Fibrothecoma
    - Sclerosing stromal tumor
  - Sertoli-stromal tumors
    - Sertoli-Leydig cell tumor
  - Steroid cell tumors
  - Other tumors
- Metastatic tumors

Epithelial Tumors

Epithelial ovarian tumors represent 60% of all ovarian neoplasms and 85% of malignant ovarian neoplasms (1,4). Epithelial tumors are rare in prepubescent patients; their prevalence increases with age and peaks in the sixth and seventh decades of life (1). Subtypes of epithelial tumors include serous, mucinous, endometrioid, clear cell, and Brenner tumors (1,4,5). Epithelial ovarian tumors can be classified as benign (60% of cases), malignant (35%), or borderline (low-malignant-potential) (5%) depending on their histologic characteristics and clinical behavior (6).

Serous versus Mucinous Tumors

Epithelial tumors are typically primarily cystic, may be either unilocular or multilocular, and, when malignant, are associated with varying proportions of solid tissue (6). The two most common types of epithelial neoplasms are serous and mucinous tumors (7). In terms of their pathologic features, disease course, and prognosis, serous and mucinous ovarian tumors are different, but clinical differentiation is not easy (6). In many instances, epithelial tumors tend to be cystic and solid at gross morphologic examination, and their cell types cannot be differentiated on the basis of their appearance at MR imaging, CT, or ultrasonography (US) (6–8). However, some features can aid in differentiating mucinous from serous tumors (Table 2) (6–10). A tumor that manifests as a unilocular or multilocular cystic mass with homogeneous CT attenuation or MR imaging signal intensity of the locules, a thin regular wall or septum, and no endocystic or exocystic vegetation is considered to be a benign serous cystadenoma (Fig 1). A tumor that manifests as a multilocular cystic mass that has a thin regular wall and septa or that contains liquids of different

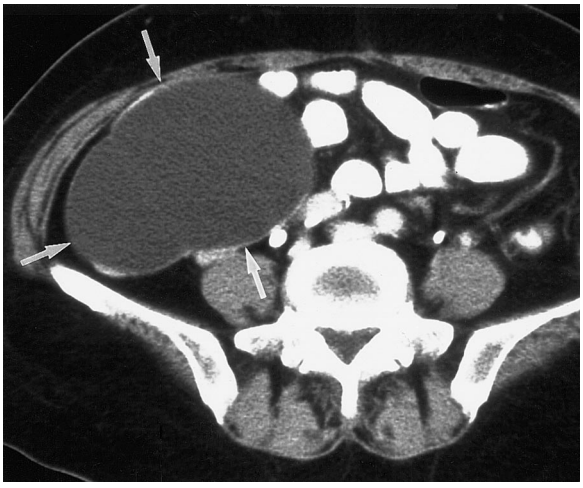

Figure 1. Benign serous cystadenoma in a 49-year-old woman. Contrast material–enhanced CT scan shows a unilocular cystic mass in the right lower quadrant (arrows). The wall of the mass is not delineated, and there is no evidence of any excrescence within it.

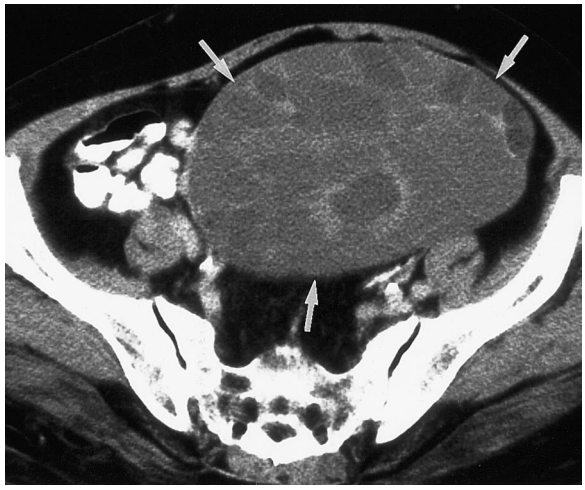

Figure 2. Benign mucinous cystadenoma in a 26-year-old woman. Contrast-enhanced CT scan shows a large, multilocular cystic mass (arrows) with a smooth contour, honeycomb appearance, and heterogeneous attenuation in the locules.

Table 2
Features that Help Differentiate Serous from Mucinous Tumors

	Tumor Type	
Feature	Serous	Mucinous
Clinical findings		
Benign ovarian tumors	25%	20%
Malignant ovarian tumors	50%	10%
Proportion of malignant cases	60% benign, 15% low malignant potential, 25% malignant	80% benign, 10%–15% low malignant potential, 5%–10% malignant
Imaging findings		
Size	Smaller than mucinous tumors	Often large; may be enormous
Wall, locule	Thin-walled cyst, usually unilocular	Multilocular, small cystic component, honeycomb-like locules
Opacity or signal intensity of locule	Stable	Variable
Papillary projections	Often seen	Rare
Calcification	Psammomatous, common	Linear, rare
Bilaterality	Frequent	Rare
Carcinomatosis	More common	Pseudomyxoma peritonei

attenuation or signal intensity but has no endocystic or exocystic vegetation is considered to be a benign mucinous cystadenoma (Fig 2). Mucinous cystadenomas tend to be larger than serous cystadenomas at presentation (6–10). About 60% of all the serous ovarian neoplasms are smooth-walled benign cystadenomas, 15% are of low malignant potential, and 25% are malignant. In contrast, 80% of all mucinous ovarian neoplasms are smooth-walled benign cystadenomas, 10%–15% are of low malignant potential, and 5%–10% are malignant (9–12). Psammoma bodies

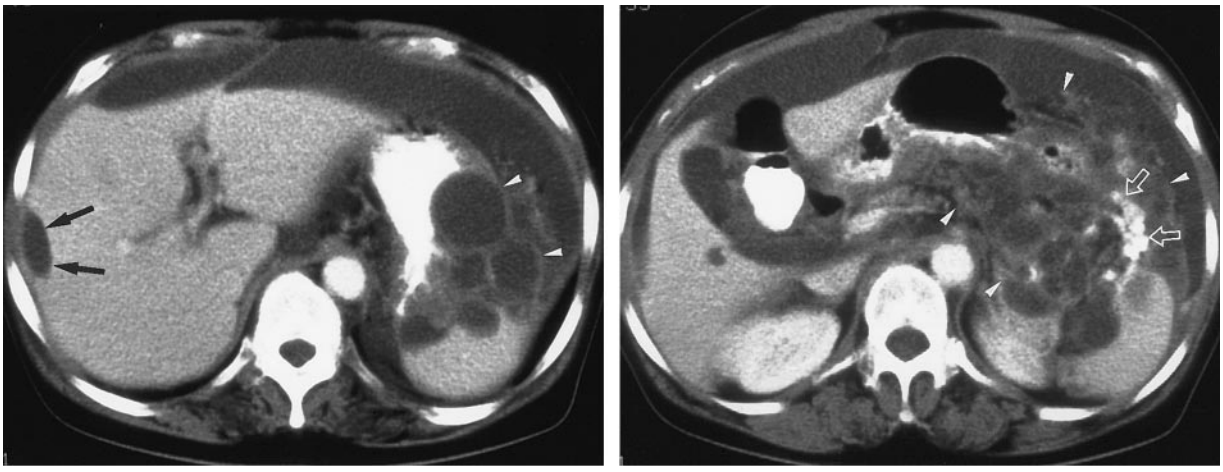

a. b.

Figure 3. Serous cystadenocarcinoma of the ovary with peritoneal carcinomatosis in a 60-year-old woman. Contrast-enhanced CT scans obtained at the level of the liver **(a)** and upper pole of the kidney **(b)** show a subcapsular hepatic implant with a scalloped margin (arrows in **a**). Diffuse multilocular cystic implants are seen along the greater omentum, parietal peritoneum, gastrosplenic ligament, and lesser sac (arrowheads), and calcified peritoneal implants are noted in the gastrosplenic ligaments (arrows in **b**). Massive ascites is also present.

(calcifications) are seen at histologic analysis in up to 30% of malignant serous tumors (6). Bilaterality and peritoneal carcinomatosis are seen more frequently in serous than in mucinous cystadenocarcinomas (Figs 3, 4) (9). Mucinous adenocarcinoma can rupture and is associated with pseudomyxoma peritonei (Fig 5) (10).

Benign versus Low-Malignant-Potential and Malignant Tumors

Benign serous and mucinous tumors are common, but benign endometrioid tumors are very rare, and all clear cell carcinomas are malignant (6). The imaging features that are more suggestive of either benignity or malignancy are summarized in Table 3 (6–13).

Features that are more suggestive of benign epithelial tumors include a diameter less than 4 cm, entirely cystic components, a wall thickness

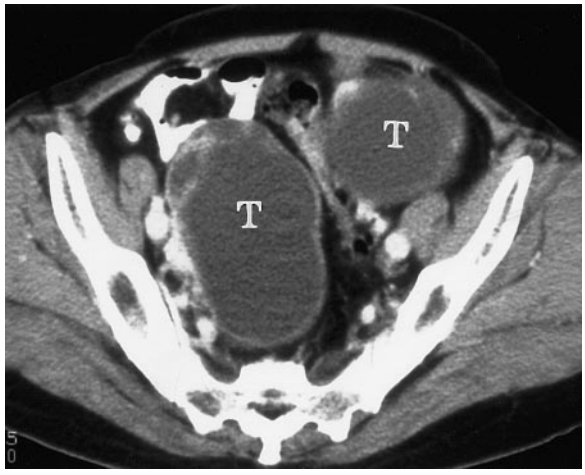

Figure 4. Bilateral serous cystadenocarcinomas in a 50-year-old woman. Contrast-enhanced CT scan shows bilateral ovoid tumors *(T)* with some septa and mural nodules.

less than 3 mm, lack of internal structure, and the absence of both ascites and invasive characteristics such as peritoneal disease or adenopathy

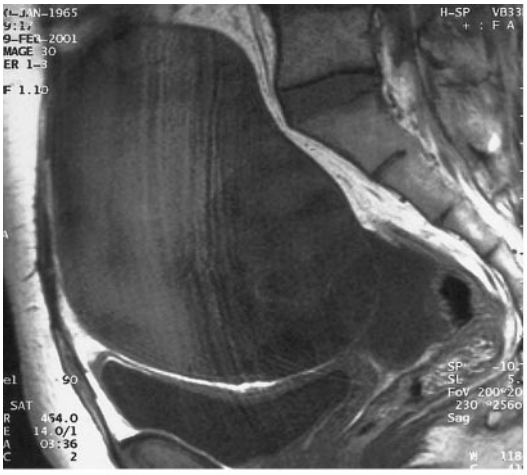

a.

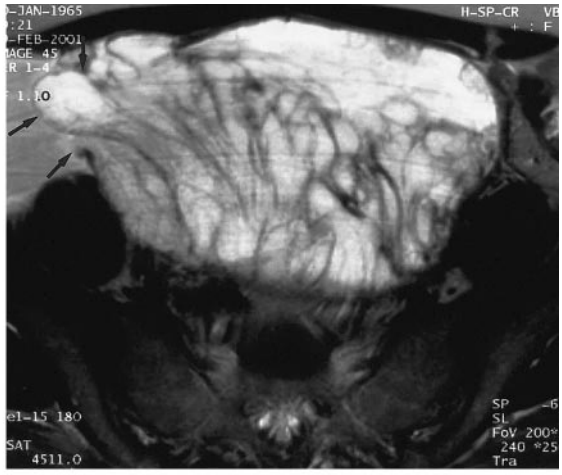

b.

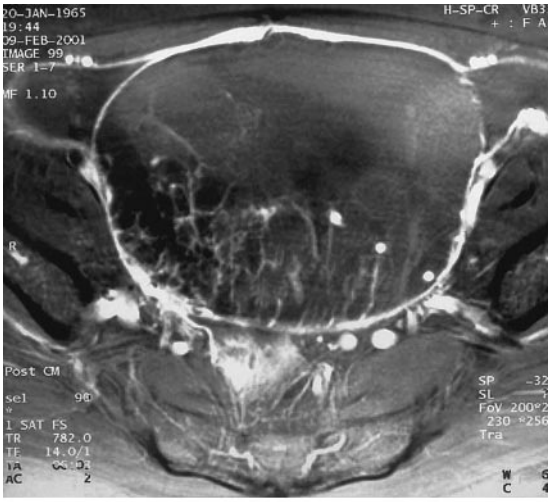

c.

Figure 5. Ruptured mucinous cystadenocarcinoma in a 36-year-old woman. **(a)** Sagittal turbo spin-echo T1-weighted MR image (repetition time msec/echo time msec = 464/14) shows a large, multilocular mass with heterogeneous high signal intensity but with variable signal intensity in the locules. **(b)** On an axial turbo spin-echo T2-weighted MR image (4,511/132), the mass demonstrates high signal intensity, and there are multiple locules with a honeycomb appearance. The tumor wall is disrupted by spillage of the mucinous material (arrows). **(c)** Gadolinium-enhanced fat-suppressed turbo spin-echo T1-weighted MR image (782/14) demonstrates marked enhancement of the tumor wall and septa.

Table 3
Features that Suggest Either Benign or Malignant Epithelial Neoplasms

	Tumor Type	
Variable	Benign	Malignant
Component	Entirely cystic	Large soft-tissue mass with necrosis
Wall thickness	Thin (less than 3 mm)	Thick
Internal structure	Lacking	Papillary projection
Ascites	None	Peritoneal, anterior to uterus
Other	. . .	Peritoneal implants, pelvic wall invasion, adenopathy

(10). Exceptionally large benign neoplasms occur are occasionally seen and are more likely to remain clinically silent as they grow (11). Epithelial tumors with low malignant potential demonstrate more proliferation of papillary projections than do benign cystadenomas (Fig 6) and are often seen in younger patients (14,15). Epithelial tumors

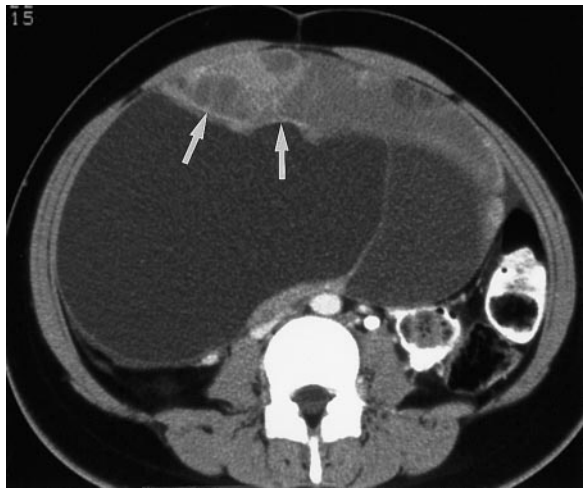

Figure 6. Borderline mucinous tumor in a 20-year-old woman. Contrast-enhanced CT scan shows a large, multilocular cystic mass with variable attenuation in the locules and enhancing solid-tissue elements (arrows).

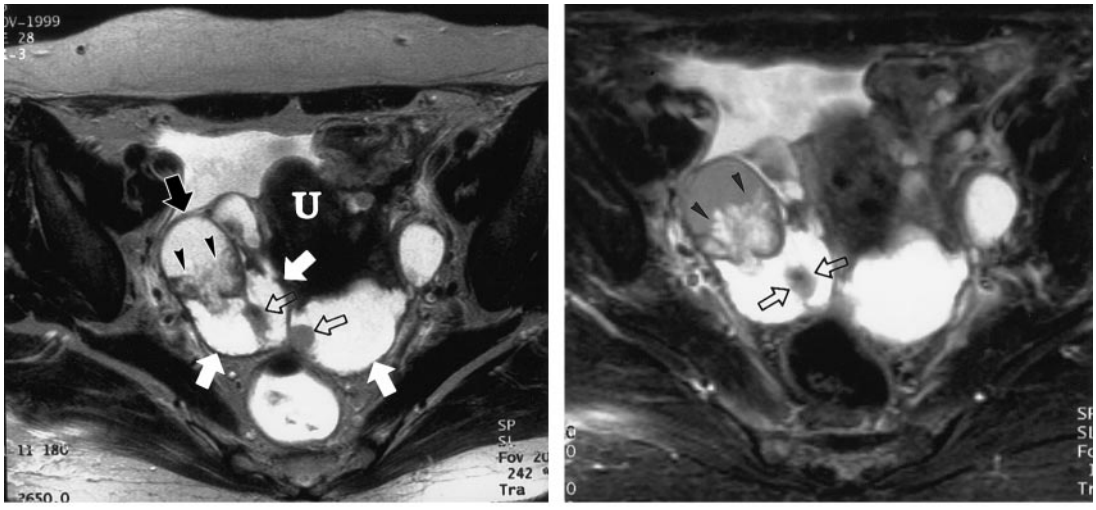

a. **b.**

Figure 7. Papillary serous cystadenocarcinoma in a 53-year-old woman. **(a)** Axial turbo spin-echo T2-weighted MR image (3,650/99) shows a multilocular mass (solid arrows) around the uterus *(U)* with irregular solid components (open arrows) and intracystic papillary projections (arrowheads). The mass consists of a low-signal-intensity fibrous core and barely visible edematous stroma. **(b)** On an axial inversion-recovery MR image (4,890/60), a high-signal-intensity edematous stroma of papillary projections (arrowheads) is clearly seen, whereas the solid component (arrows) has low signal intensity. **(c)** Sagittal gadolinium-enhanced fat-suppressed turbo spin-echo T1-weighted MR image (905/12) shows marked enhancement of the papillary projections (arrowheads) and solid component (arrow) but less enhancement of the fibrous components.

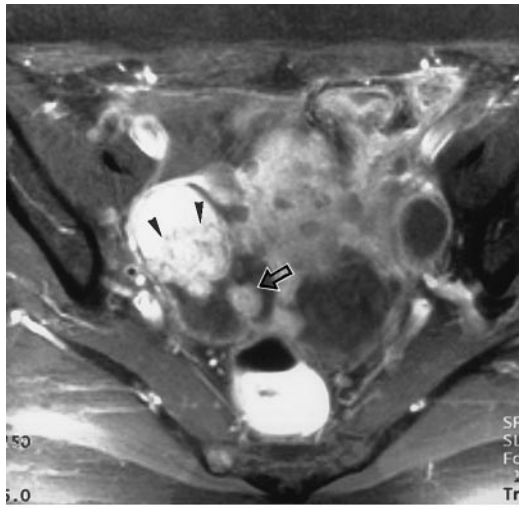

c.

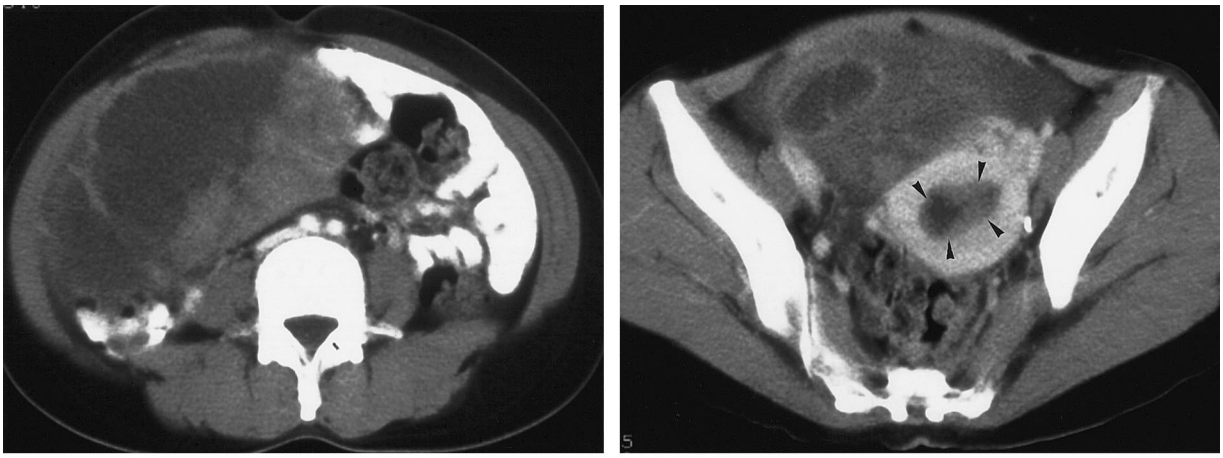

a. b.

Figure 8. Endometrioid carcinoma of the ovary and endometrial carcinoma of the uterus in a 38-year-old woman. **(a)** Contrast-enhanced lower abdominal CT scan shows a complex cystic and solid tumor with enhancement of the solid-tissue elements and a thick, irregular wall. **(b)** Contrast-enhanced pelvic CT scan shows a widened endometrial cavity with a nodular enhancing solid mass (arrowheads).

with low malignant potential have a much better prognosis than do ovarian carcinomas. They offer the potential for ovarian-uterine–sparing surgery and have less frequent indications for adjuvant chemotherapy; however, like carcinomas, they require initial staging surgery (16,17).

Papillary projections are characteristic features of some epithelial neoplasms of the ovary. Histologically, papillary projections represent folds of the proliferating neoplasmic epithelium growing over a stromal core. T2-weighted MR images demonstrate the structure of a hypointense fibrous core that supports the hyperintense edematous stroma (Fig 7) (7,16). Identification of papillary projections on an imaging study is important because they are the single best predictors of an epithelial neoplasm and may correlate with the aggressiveness of the tumor. Papillary projections are usually absent in benign cystadenomas; if they are present, they are generally small. Papillary projections are profuse in epithelial tumors with low malignant potential and are often present in invasive carcinomas, but the gross appearance of the tumor is dominated by a solid component. A previous CT and MR imaging study found papillary projections in 13% of benign neoplasms, 67% of low-malignant-potential neoplasms, and 38% of malignant neoplasms (16).

Imaging findings that are suggestive of malignant tumors include a thick, irregular wall; thick septa; papillary projections; and a large soft-tissue component with necrosis (10). Ancillary findings of pelvic organ invasion, implants (peritoneal, omental, mesenteric), ascites, and adenopathy increase diagnostic confidence for malignancy (Fig 3) (7). Features such as wall thickening, septa, and multilocularity are less reliable indicators of malignancy because they are frequently seen in benign neoplasms, particularly cystadenofibromas, mucinous cystadenomas, and endometriomas (17).

Endometrioid Carcinoma

Endometrioid carcinomas represent approximately 10%–15% of all ovarian carcinomas. They are almost always malignant. About 15%–30% are associated with synchronous endometrial carcinoma or endometrial hyperplasia (11,12). Although rare, endometrioid carcinoma is the most common malignant neoplasm arising from endometriosis, followed by clear cell carcinoma (18,19). Bilateral involvement is seen in 30%–50% of cases (11,12). Imaging findings are nonspecific and include a large, complex cystic mass with solid components. Endometrial thickening can also be seen on imaging studies (Fig 8) (6).

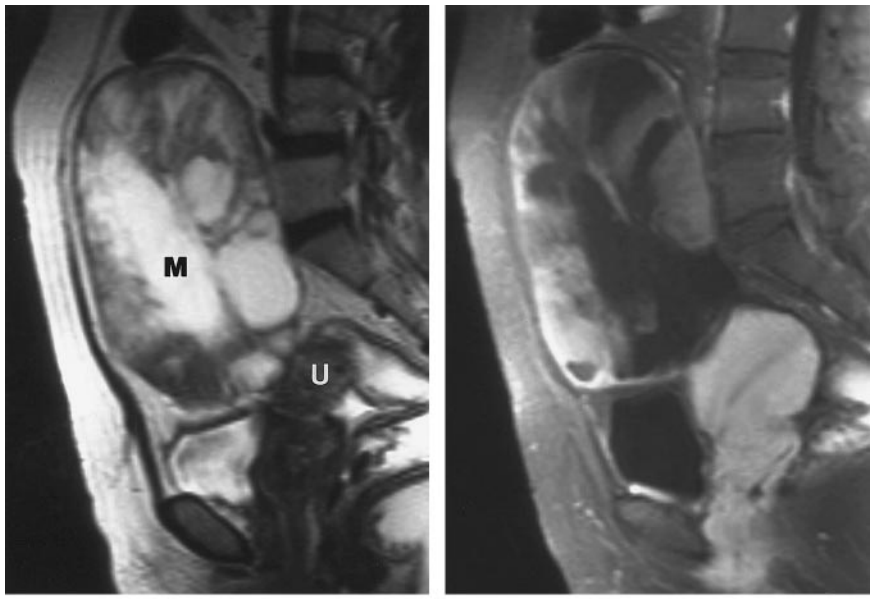

Figure 9. Clear cell carcinoma in a 42-year-old woman. **(a)** Sagittal turbo spin-echo T2-weighted MR image (4,275/138) demonstrates a large cystic mass *(M)* with hypointense, irregular solid protrusions peripherally. *U* = uterus. **(b)** Gadolinium-enhanced fat-suppressed fast low-angle shot (FLASH) T1-weighted MR image (147/4.8) demonstrates marked enhancement of the solid portions of the mass.

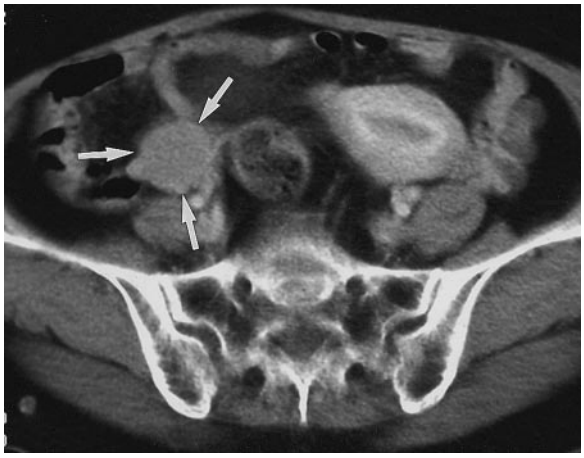

Figure 10. Incidentally discovered Brenner tumor in a 68-year-old woman. Contrast-enhanced CT scan shows a small, ovoid solid mass with homogeneous enhancement (arrows), a finding that is nonspecific for a solid tumor.

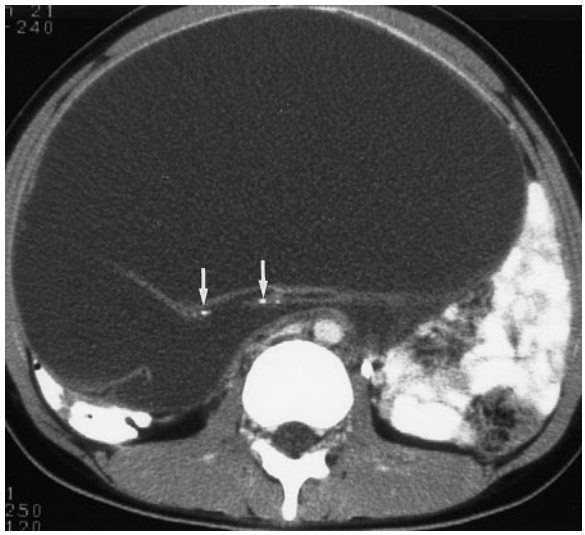

Figure 11. Atypical mature teratoma with a purely cystic component in a 16-year-old girl. Contrast-enhanced CT scan shows a large cystic mass with multiple septa, one of which contains calcifications (arrows). There is no evidence of a fatty component.

Clear Cell Carcinoma

Clear cell carcinomas represent approximately 5% of ovarian carcinomas and are always malignant (12). The majority (75%) of clear cell carcinomas are stage I disease whose prognosis appears to be better than that of other ovarian cancers (20,21). Clear cell carcinoma may develop in patients with endometriosis who develop ovarian cancer. A large endometrioma with solid components suggests malignancy and must be removed (11,12). Common imaging findings in clear cell carcinoma include a unilocular or large cyst with solid protrusions (Fig 9). The cyst margin is almost always smooth, and its signal intensity on

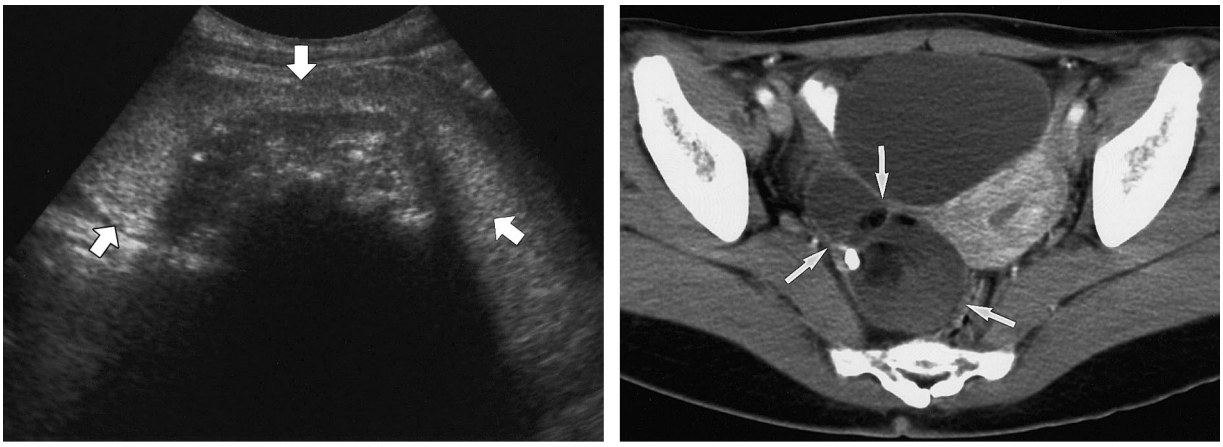

a. b.

Figure 12. Mature teratoma in a 22-year-old woman. **(a)** Axial US image demonstrates a mostly echogenic mass (arrows) with areas of sound attenuation. **(b)** Contrast-enhanced CT scan shows a cystic tumor with fat and calcification (arrows).

T1-weighted MR images varies from low to very high. The solid protrusions are often both round and few in number (21). These findings suggest, but are not specific for, malignant tumor. Although these findings most likely indicate a serous tumor with low malignant potential or a serous cystadenocarcinoma, the differential diagnosis should include clear cell carcinoma.

Brenner Tumor

Brenner tumors are composed of transitional cells with dense stroma. They represent about 2%–3% of ovarian tumors and are rarely malignant. Brenner tumors are usually small (<2 cm) and discovered incidentally, but affected patients may present with a palpable mass or pain. Brenner tumors are associated with other ovarian tumors in 30% of cases (8,22,23).

Brenner tumors manifest as a multilocular cystic mass with a solid component or as a small, mostly solid mass (Fig 10). At CT, the solid components of these masses are mildly or moderately enhanced. At T2-weighted MR imaging, the dense fibrous stroma demonstrates lower signal intensity similar to that of a fibroma. Extensive amorphous calcification is often present within the solid component (22,23).

Germ Cell Tumors

Tumors of germ cell origin are the second most common group of ovarian neoplasms, representing 15%–20% of all ovarian tumors. This group of tumors includes mature teratoma, immature teratoma, dysgerminoma, endodermal sinus tumor, embryonal carcinoma, and choriocarcinoma (9,24). Of all the germ cell tumors, only mature teratoma is benign; however, it is by far the most common lesion in this group. All the other tumors are malignant and account for less than 5% of malignant ovarian tumors. Malignant germ cell tumors are generally large and nonspecific with a complex but predominantly solid imaging appearance. Elevated levels of serum α-fetoprotein and human chorionic gonadotropin (HCG) can also help establish the diagnosis (24–26).

Mature Teratoma

Mature teratoma is the most common benign ovarian tumor in women less than 45 years old. These teratomas are composed of mature tissue from two or more embryonic germ cell layers. At gross pathologic examination, mature cystic teratomas are unilocular, and in 88% of cases, they are filled with sebaceous material and lined by squamous epithelium (25). Hair follicles, skin glands, muscle, and other tissues lie within the wall. There is usually a raised protuberance projecting into the cyst cavity known as the Rokitansky nodule. Most of the hair typically arises from this protuberance. When bone or teeth are present, they tend to be located within this nodule (25,26).

At any imaging modality, mature teratomas demonstrate a broad spectrum of findings, ranging from purely cystic (Fig 11), to a mixed mass with all the components of the three germ cell layers (Figs 12, 13), to a noncystic mass composed predominantly of fat (Fig 14).

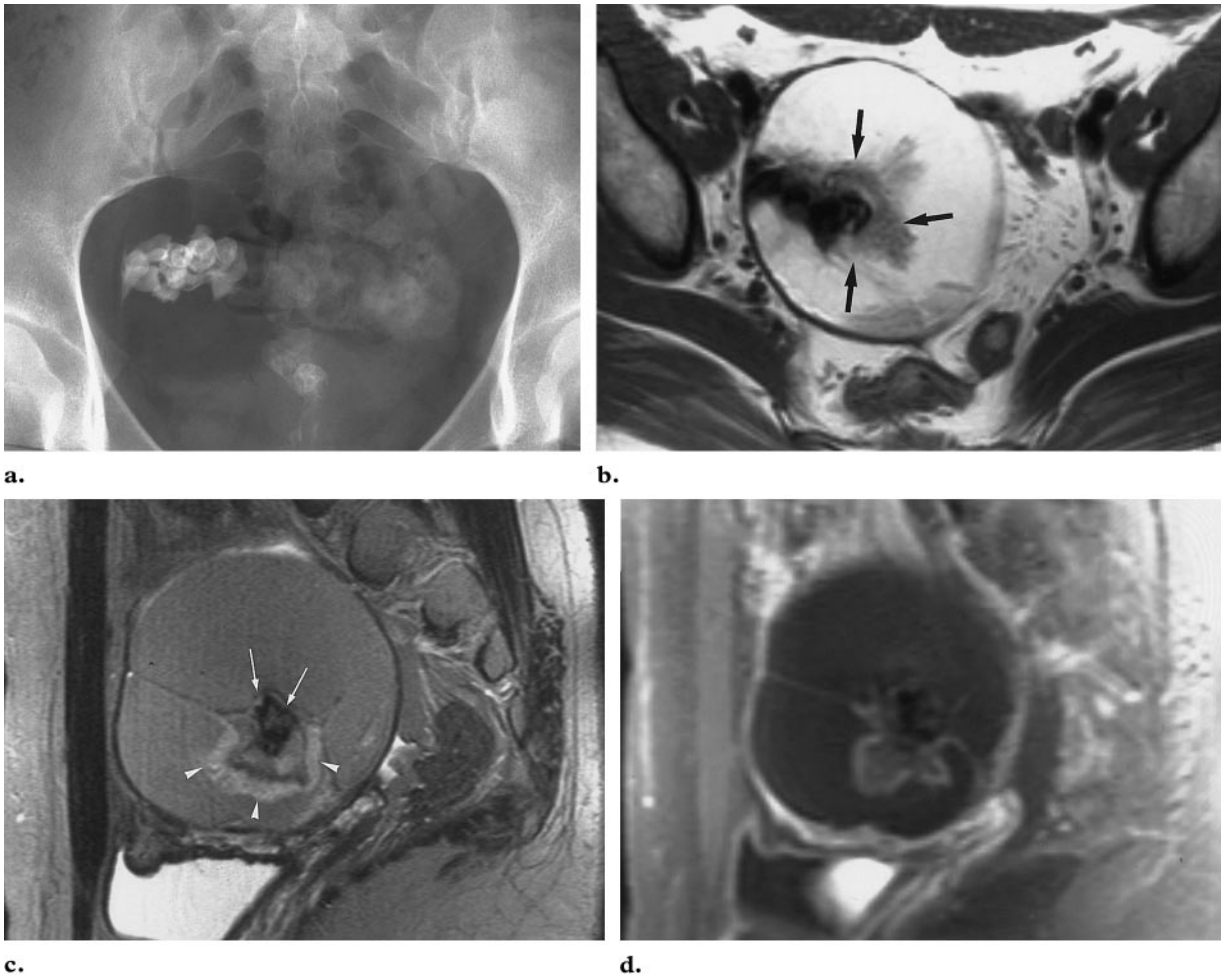

Figure 13. Mature teratoma in a 21-year-old woman. **(a)** Conventional radiograph shows a large mass with fat opacity and multiple toothlike calcifications, findings that indicate a typical mature teratoma. **(b)** Axial turbo spin-echo T1-weighted MR image (800/12) shows a well-defined round, hyperintense mass with hypointense calcifications and a mural nodule (arrows). **(c)** On a sagittal turbo spin-echo T2-weighted MR image (3,800/99), the tumor is isointense relative to subcutaneous fat. The calcifications have low signal intensity (arrows), whereas the Rokitansky protuberance has high signal intensity (arrowheads). **(d)** Gadolinium-enhanced fat-suppressed FLASH T1-weighted MR image (147/4.8) demonstrates the mass with markedly decreased signal intensity compared with the non–fat-suppressed T1-weighted image (cf **b**).

US findings in mature cystic teratomas vary from a cystic lesion with a densely echogenic tubercle (Rokitansky nodule) projecting into the cyst lumen, to a diffusely or partially echogenic mass with the echogenic area usually demonstrating sound attenuation owing to sebaceous material and hair within the cyst cavity (Fig 12), to multiple thin, echogenic bands caused by hair in the cyst cavity (26–28). The dermoid plug is echogenic, with shadowing due to adipose tissue or calcifications within the plug or to hair arising from it (26). At CT, fat attenuation within a cyst, with or without calcification in the wall, is diagnostic for mature cystic teratoma (Fig 12b) (29, 30). At MR imaging, the sebaceous component of dermoid cysts has very high signal intensity on T1-weighted images similar to that of retroperi-

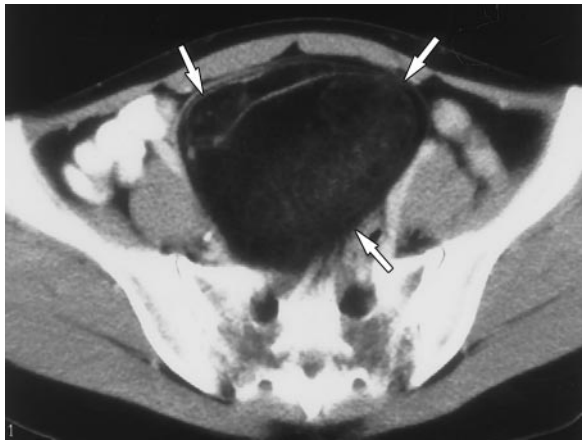

Figure 14. Mature teratoma with a mainly fatty component in a 36-year-old woman. Contrast-enhanced CT scan shows a large, fatty mass in the pelvic cavity (arrows). Mature teratomas demonstrate a wide spectrum of imaging findings because they are composed of three germ cell layers.

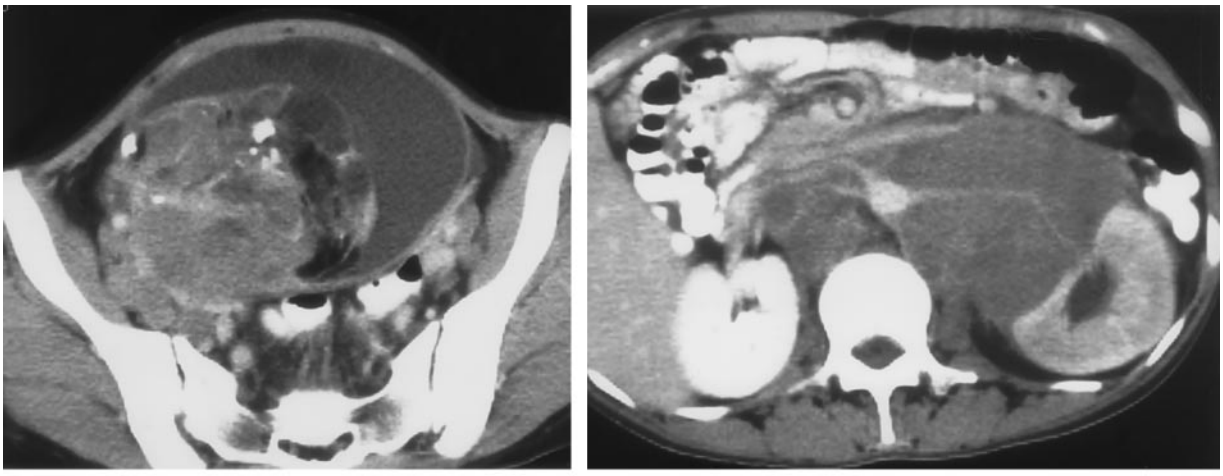

a. b.

Figure 15. Immature teratoma in a 23-year-old woman. **(a)** Contrast-enhanced pelvic CT scan shows a large mass with a large soft-tissue component, a cystic portion, small foci of fat, and scattered calcifications. **(b)** CT scan obtained at the level of the renal hilum demonstrates extensive retroperitoneal adenopathy.

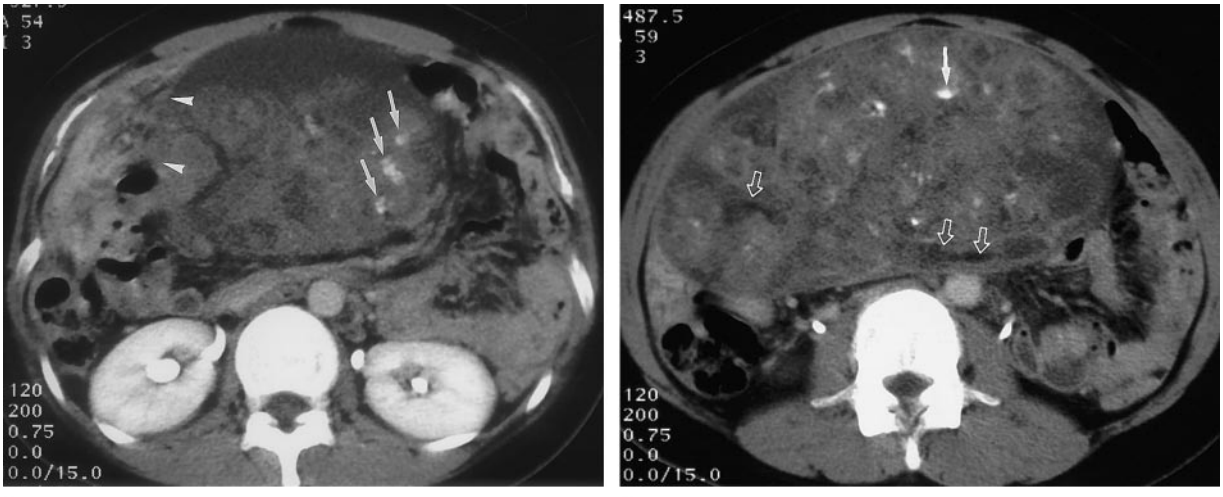

a. b.

Figure 16. Ruptured immature teratoma in a 19-year-old woman. Contrast-enhanced CT scans obtained at the level of the renal hilum **(a)** and midabdomen **(b)** show a large, heterogeneous mass with scattered calcifications (solid arrows) and foci of fat (open arrows in **b**). Perforation of the capsule (arrowheads in **a**) and tumor in the peritoneum are both present.

toneal fat. The signal intensity of the sebaceous component on T2-weighted images is variable, usually near that of fat (Fig 13c) (26,30).

Mature cystic teratoma may be associated with complications from torsion, rupture, or malignant degeneration (26,31). The tumors can rupture, causing leakage of the liquefied sebaceous contents into the peritoneum and resulting in granulomatous peritonitis (26). Less common forms of mature teratomas are the monodermal types, which include struma ovarii (in which mature thyroid tissue predominates) and carcinoids (26).

Immature Teratoma

Immature teratoma represents less than 1% of all teratomas and contains immature tissue from all three germ cell layers (24,26). The tumor strikes during the first 2 decades of life. Benign mature teratomas must be differentiated from malignant, immature teratomas, which have prominent solid components and may demonstrate internal necrosis or hemorrhage. Mature tissue elements similar to those seen in mature cystic teratoma are invariably present (Fig 15) (24,26). Radiologic examination reveals a large, complex mass with cystic and solid components and scattered calcifications; in contrast, calcification in mature teratomas is localized to mural nodules (24). Small foci of fat are also seen in immature teratomas. These tumors grow rapidly and frequently demonstrate perforation of the capsule. The tumor capsule is not always well defined (Fig 16) (26).

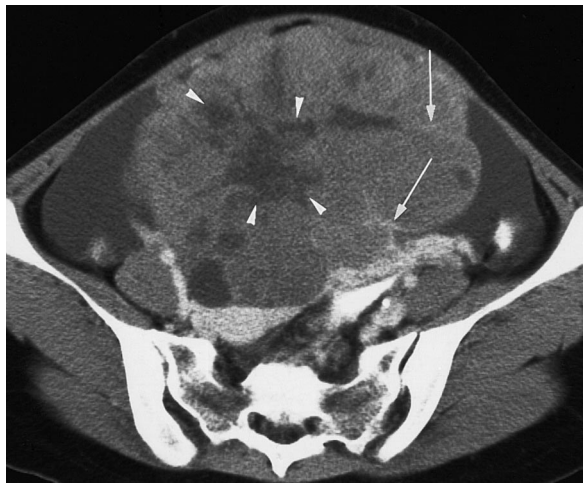

Figure 17. Dysgerminoma in an 18-year-old woman. Contrast-enhanced CT scan shows a large, multilobulated solid mass with highly enhancing fibrovascular septa (arrows) and cystic change (arrowheads).

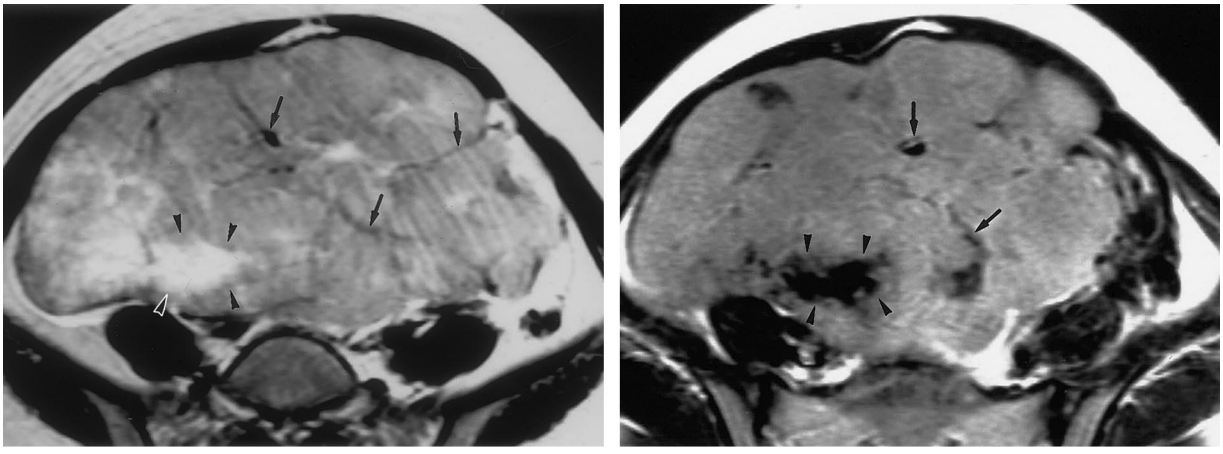

a. **b.**

Figure 18. Dysgerminoma in a 17-year-old girl. **(a)** Axial turbo spin-echo T2-weighted MR image (3,800/99) shows a large, multilobulated mass with intermediate signal intensity and persistent low signal intensity of the septa (arrows). The irregular high-signal-intensity areas (arrowheads) indicate necrosis. **(b)** Axial gadolinium-enhanced turbo spin-echo T1-weighted MR image (782/14) demonstrates relatively homogeneous enhancement with persistent low signal intensity of the septa (arrows) and unenhanced necrotic areas (arrowheads).

Dysgerminoma

Dysgerminomas are rare ovarian tumors that occur predominantly in young women. This tumor is the ovarian counterpart of seminoma of the testis (24). Dysgerminoma in its pure form is not associated with endocrine hormone secretion. However, syncytiotrophoblastic giant cells, which produce HCG, are present in 5% of dysgerminomas and can cause elevation of serum HCG levels. Calcification may be present in a speckled pattern (32). Characteristic imaging findings include multilobulated solid masses with prominent fibrovascular septa (Fig 17). The anechoic, low-signal-intensity, or low-attenuation area of the tumor represents necrosis and hemorrhage (Fig 18) (32,33).

Endodermal Sinus Tumor

Endodermal sinus tumor, also known as yolk sac tumor, is a rare malignant ovarian tumor that usually occurs in the second decade of life (24).

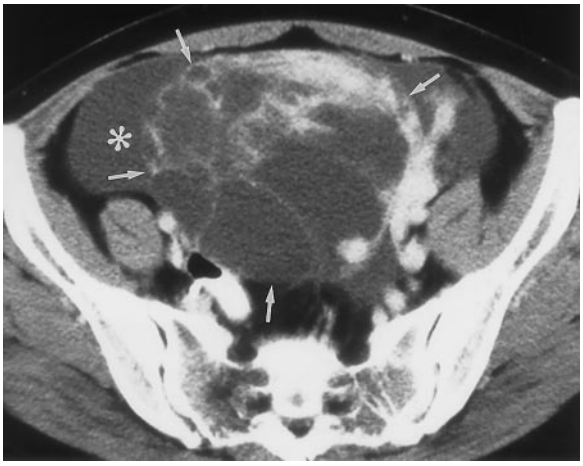

Figure 19. Endodermal sinus tumor in a 29-year-old woman. Contrast-enhanced CT scan shows a large, complex pelvic mass with solid and cystic components (arrows). Associated ascites is also seen (*). The patient had an elevated serum α-fetoprotein level of 58,000 IU/mL (normal range, 0–15 IU/mL).

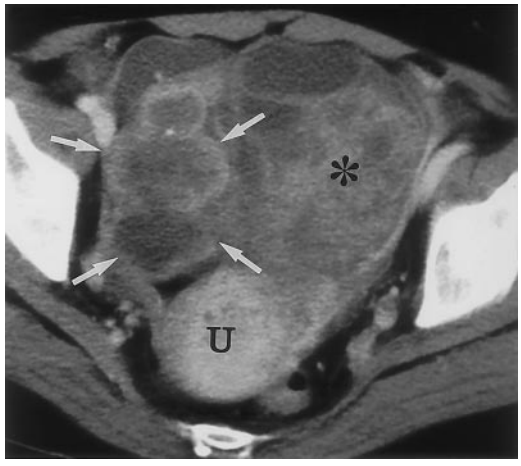

Figure 20. Granulosa cell tumor in a 55-year-old woman. Contrast-enhanced CT scan shows a large, complex mass with a lobular contour, multiple cysts with a "bunch of grapes" appearance on the right (arrows), and an irregularly enhancing solid portion on the left (*). *U* = uterus.

The tumor manifests as a large, complex pelvic mass that extends into the abdomen and contains both solid and cystic components (Fig 19). The cystic areas are composed of epithelial line cysts produced by the tumor or of coexisting mature teratomas. These tumors grow rapidly and have a poor prognosis. Affected patients have an elevated serum α-fetoprotein level (34,35).

Sex Cord–Stromal Tumors

Gonadal cell types that derive from the coelomic epithelium (sex cords) or mesenchymal cells of the embryonic gonads include granulosa cells, theca cells, fibroblasts, Leydig cells, and Sertoli cells. Ovarian tumors composed of these cell types are called sex cord–stromal tumors (Table 1). This group of tumors represents approximately 8% of ovarian neoplasms and affects all age groups. The most common types are granulosa cell tumors, fibrothecomas, and Sertoli-Leydig cell tumors. Sex cord–stromal tumors are of interest partly because of their hormonal effects, which are rare in other ovarian neoplasms (36). The vast majority of sex cord–stromal tumors are either benign (eg, fibrothecoma, sclerosing stromal tumor) or largely confined to the ovary at diagnosis (eg, granulosa cell tumor, Sertoli-Leydig cell tumor) (36).

Granulosa Cell Tumor

Granulosa cell tumor of the ovary is the most common malignant sex cord–stromal tumor as well as the most common estrogen-producing ovarian tumor. Adult granulosa cell tumors are far more common than the juvenile type and account for 95% of all granulosa cell tumors. They occur predominantly in peri- and postmenopausal women. The hyperestrogenemia may produce combined endometrial hyperplasia, polyps, or carcinoma. Endometrial carcinoma is associated with these neoplasms in 3%–25% of cases (36–39). Imaging findings in adult ovarian granulosa cell tumors vary widely and range from solid masses, to tumors with varying degrees of hemorrhagic or fibrotic changes, to multilocular cystic lesions (Fig 20), to completely cystic tumors. Intratumoral bleeding, infarcts, fibrous degeneration, and irregularly arranged tumor cells have yielded heterogeneously solid tumors (37,38). In contrast with epithelial neoplasms, granulosa cell tumors do not have intracystic papillary projections, have less propensity for peritoneal seeding, and are confined to the ovary at the time of diagnosis. Estrogenic effects on the uterus may manifest as uterine enlargement or as endometrial thickening or hemorrhage (Fig 21) (36).

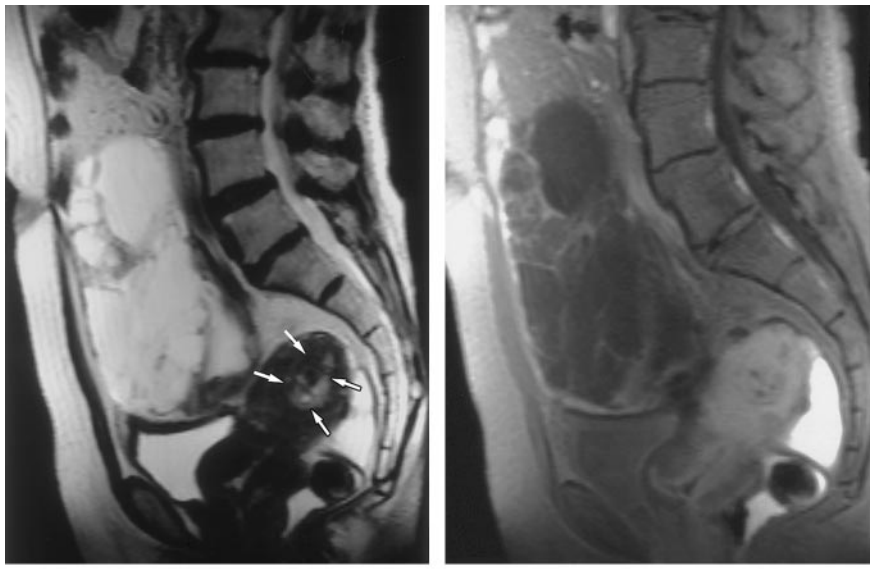

a. b.

Figure 21. Granulosa cell tumor in a 71-year-old woman. **(a)** Sagittal turbo spin-echo T2-weighted MR image (4,275/138) shows a lobulated multilocular cystic mass that resembles a cystadenocarcinoma. However, no evidence of a papillary projection is noted. The endometrial cavity (arrows) is unusually prominent for a patient this age, a finding that is consistent with endometrial hyperplasia. **(b)** Gadolinium-enhanced fat-suppressed FLASH T1-weighted MR image (148/4.8) demonstrates multiple well-enhanced septa, with numerous large cystic spaces lined by granulosa cells. These findings represent an extreme example of the macrofollicular pattern.

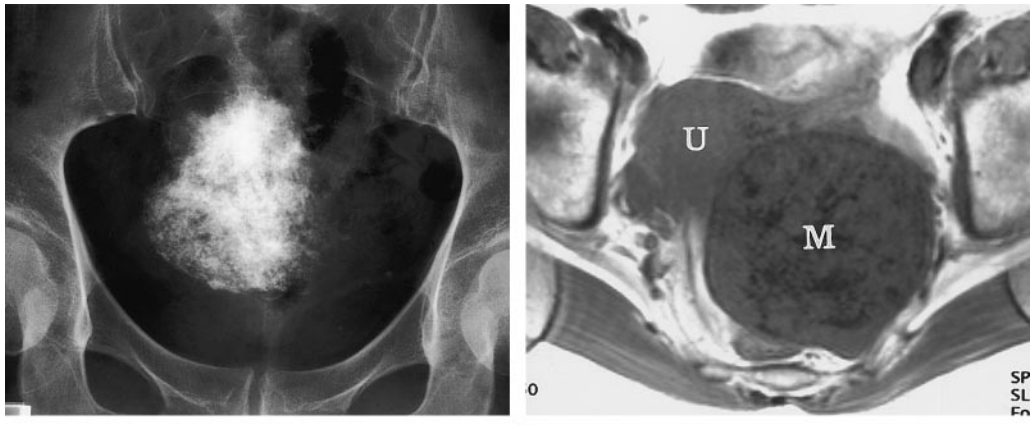

a. b.

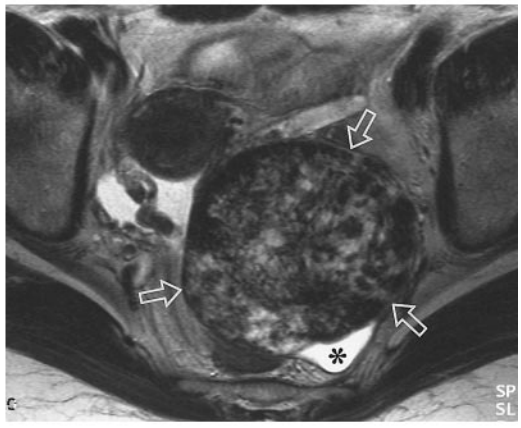

c.

Figure 22. Fibroma in a 53-year-old woman. **(a)** Conventional radiograph shows dense amorphous calcification in the pelvic cavity. The initial diagnosis was leiomyoma with dystrophic calcification. **(b)** Axial turbo spin-echo T1-weighted MR image (800/12) shows a well-defined round mass *(M)* with extensive low-signal-intensity foci representing calcifications. *U* = uterus. **(c)** On an axial turbo spin-echo T2-weighted MR image (5,200/132), the mass (arrows) has low signal intensity with high-signal-intensity foci. A small amount of ascites is present in the cul-de-sac (*).

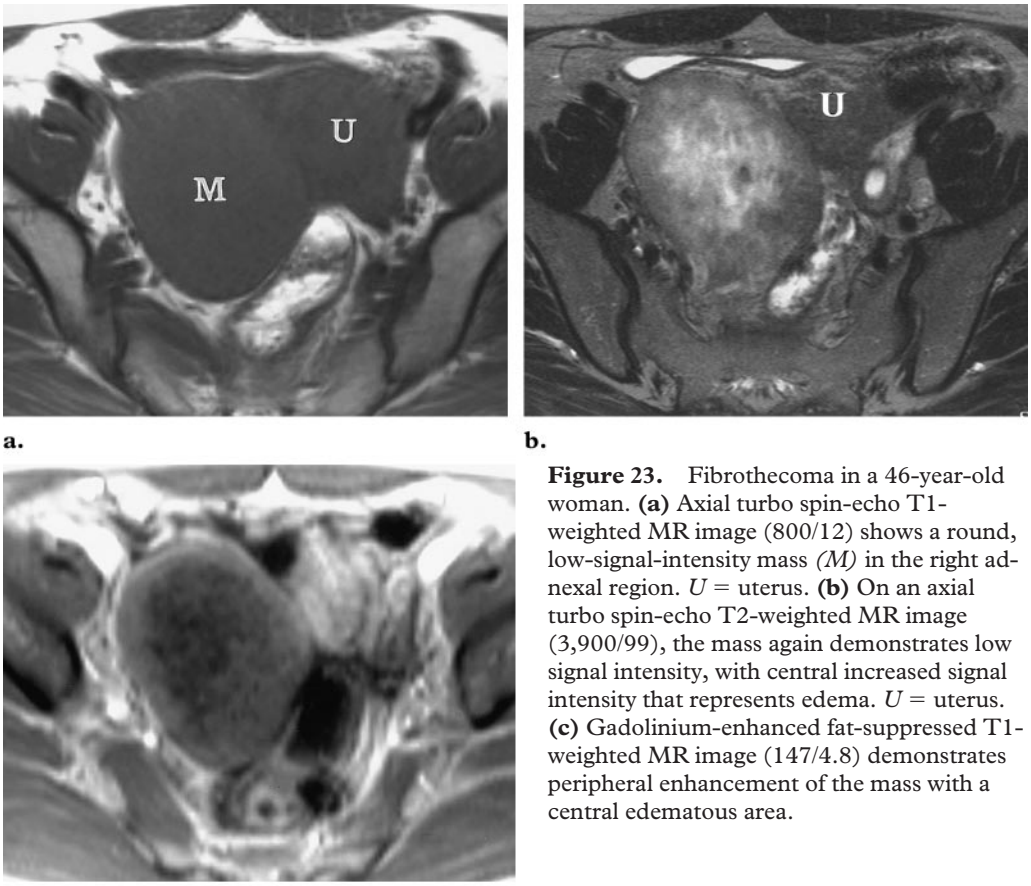

a. b. c.

Figure 23. Fibrothecoma in a 46-year-old woman. **(a)** Axial turbo spin-echo T1-weighted MR image (800/12) shows a round, low-signal-intensity mass *(M)* in the right adnexal region. *U* = uterus. **(b)** On an axial turbo spin-echo T2-weighted MR image (3,900/99), the mass again demonstrates low signal intensity, with central increased signal intensity that represents edema. *U* = uterus. **(c)** Gadolinium-enhanced fat-suppressed T1-weighted MR image (147/4.8) demonstrates peripheral enhancement of the mass with a central edematous area.

Fibrothecoma

Fibroma and thecoma are forms of a spectrum of benign tumors. Lipid-rich thecoma demonstrates estrogenic activity and few fibroblasts. In contrast, fibroma has no thecal cells and demonstrates no estrogenic activity. These tumors occur in both pre- and postmenopausal women. Fibroma is the most common sex cord tumor. It is composed of whorled bundles of cytologically bland, benign, spindle-shaped fibroblasts and collagen (36,40). Ovarian fibromas are important from an imaging standpoint because they appear as solid masses, thereby mimicking malignant neoplasms. They are associated with ascites or Meigs syndrome (7,9). US demonstrates a homogeneous hypoechoic mass with posterior acoustic shadowing. However, a broad spectrum of US features is seen, and in most cases the appearance of the tumor is nonspecific (41). CT shows a homogeneous solid tumor with delayed enhancement (42). Because of their abundant collagen contents, these tumors have low signal intensity on T1-weighted MR images and very low signal intensity on T2-weighted images (Fig 22). These findings are relatively diagnostic for fibroma (40). Dense calcifications are often seen (Fig 22). Scattered high-signal-intensity areas in the mass represent edema or cystic degeneration (Fig 23) (40,42).

Ovarian masses with fibrous components include fibroma, fibrothecoma, cystadenofibroma, and Brenner tumor. The fibrous components of these masses tend to have very low signal intensity on T2-weighted MR images (7,9). Pedunculated uterine leiomyomas and broad-ligament leiomyomas frequently appear as adnexal or ovarian masses, typically with very low signal intensity on T2-weighted MR images. Subserosal myomas are supplied by the vessels from the uterine arteries that course through the adjacent myometrium and may appear as the vessels that intervene between a myoma and the adjacent uterus. In contrast, ovarian masses are most likely fed directly by the ovarian arteries or by the ovarian branches

of the uterine arteries that course along the fallopian tubes. Observation of the interface vessels between the uterus and adnexal masses seems to be useful in differentiating leiomyoma from ovarian fibroma (Fig 24) (43,44).

Sclerosing Stromal Tumor

Sclerosing stromal tumors are rare benign ovarian tumors that occur predominantly in young women (second and third decades of life in 80% of cases) (45). Imaging findings include a large mass with hyperintense cystic components and a heterogeneous solid component with intermediate to high signal intensity on T2-weighted MR images. On dynamic contrast-enhanced images, the tumors demonstrate early peripheral enhancement with centripetal progression (Fig 25). Striking early enhancement reflects the cellular areas with their prominent vascular network, and an area of prolonged enhancement in the inner portion of the mass represents the collagenous hypocellular area. These findings can be useful in differentiating sclerosing stromal tumor from fibroma by indicating the absence of contrast enhancement or slight early enhancement as well as the delayed accumulation of contrast material on dynamic contrast-enhanced images (45–47).

Sertoli-Leydig Cell Tumor

Sertoli-Leydig cell tumors occur in young women (<30 years of age) and are considered to be a low-grade malignancy. These tumors constitute 0.5% of ovarian tumors and are the most common virilizing tumor. However, only 30% of these tumors are hormonally active. The tumor is composed of heterologous tissue (eg, carcinoid, mesenchymal, and mucinous epithelial tissues) (36) and manifests as a well-defined, enhancing solid mass with intratumoral cysts (Fig 26). Signal intensity at MR imaging reflects the extent of fibrous stroma (36,48).

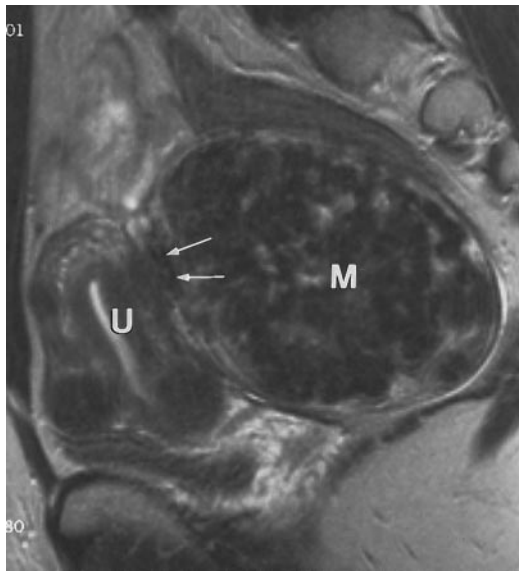

Figure 24. Subserosal leiomyoma with interface vessels in a 28-year-old woman. Sagittal turbo spin-echo T2-weighted MR image (5,200/132) shows a mass with very low signal intensity *(M)* at the posterior aspect of the uterus *(U)* and interface vessels (arrows) that resemble multiple signal void structures.

Collision Tumors

Collision tumor represents the coexistence of two adjacent but histologically distinct tumors with no histologic admixture at the interface. Ovarian collision tumors are rare. They are most commonly composed of teratoma and cystadenoma or cystadenocarcinoma (49). However, other histologic combinations have also been reported (eg, teratoma and granulosa cell tumor, cystadenocarcinoma and sarcoma) (50,51). The mechanism for the development of collision tumor is uncertain. When an ovarian tumor demonstrates imaging findings that cannot be subsumed under one histologic type, especially in cases of ovarian teratoma, a collision tumor should be considered (Fig 27) (49).

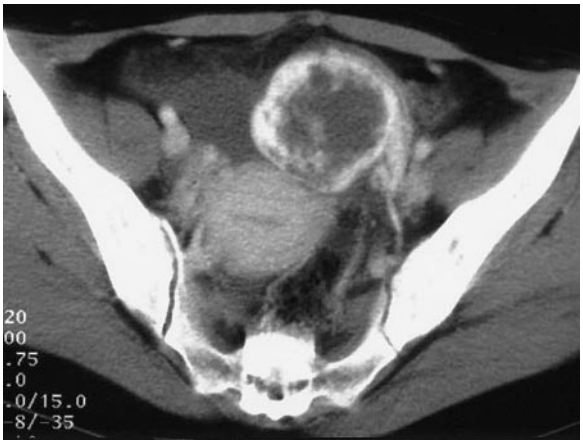

Figure 25. Sclerosing stromal tumor in a 28-year-old woman. Contrast-enhanced CT scan shows a well-defined round mass with strong peripheral enhancement anterior to the uterus.

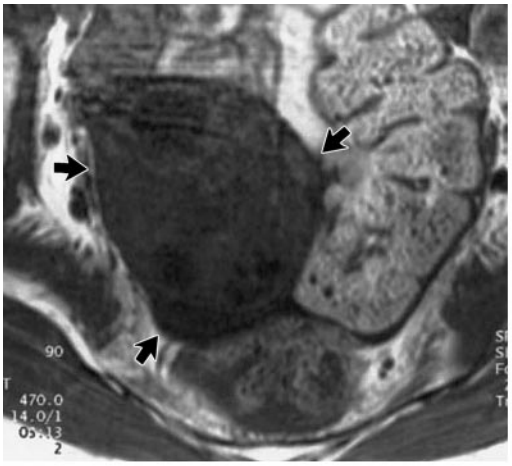

a.

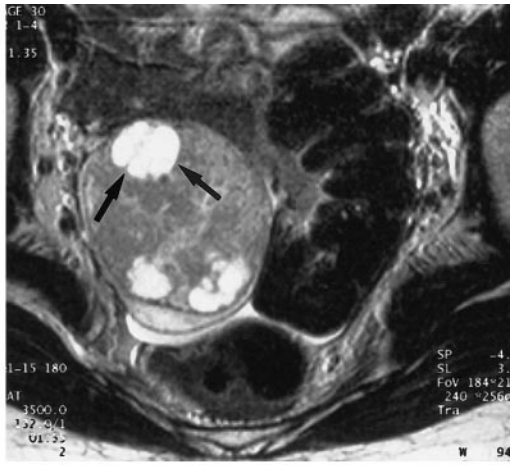

b.

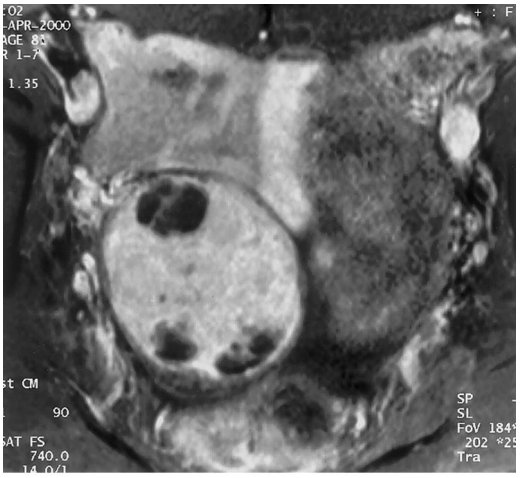

c.

Figure 26. Sertoli-Leydig cell tumor in a 23-year-old woman. **(a)** Axial turbo spin-echo T1-weighted MR image (800/12) shows a well-defined, ovoid solid mass with low signal intensity (arrows). **(b)** Axial turbo spin-echo T2-weighted MR image (3,500/132) shows the mass with intermediate signal intensity and multiple round internal cysts (arrows). **(c)** Gadolinium-enhanced fat-suppressed turbo spin-echo T1-weighted image (740/14) demonstrates the mass with a well-enhanced solid portion.

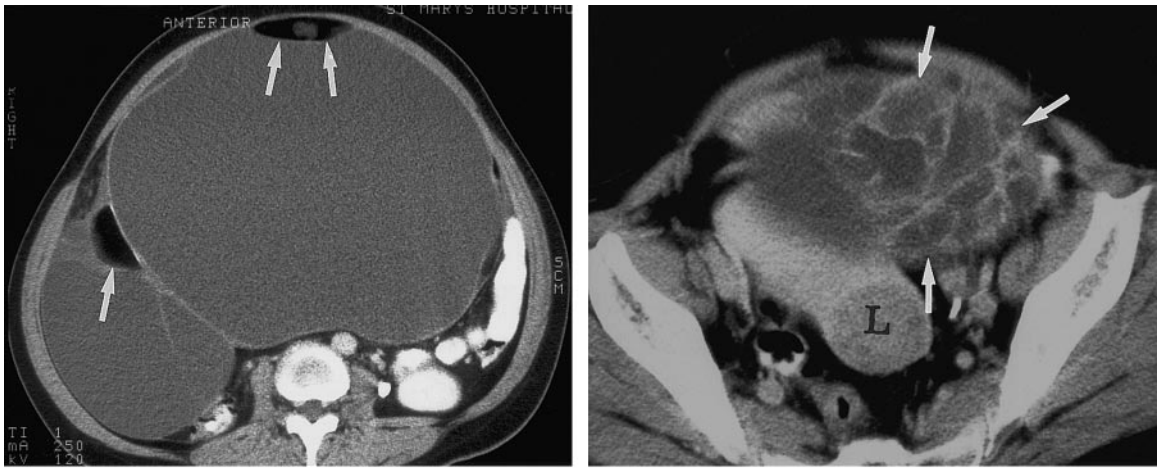

a. b.

Figure 27. Collision tumor (teratoma and mucinous cystadenoma) in a 46-year-old woman. **(a)** Contrast-enhanced CT scan of the midportion of the mass shows a typical teratoma that contains fat (arrows). **(b)** Pelvic CT scan shows a multilocular cystic tumor (arrows), a finding that indicates a mucinous cystadenoma. A small leiomyoma of the uterus *(L)* was incidentally discovered.

Metastatic Ovarian Tumors

The colon and stomach are the most common primary tumor sites in ovarian metastasis, followed by the breast, lung, and contralateral ovary. The tumors represent 10% of all ovarian tumors and develop during the reproductive years (52). Krukenberg tumors are metastatic tumors to the ovary that contain mucin-secreting "signet ring" cells and usually originate in the gastrointestinal tract (53). Differentiation between primary and metastatic ovarian carcinoma is of great importance with respect to treatment and prognosis. There are a variety of metastatic carcinomas to the ovary that can mimic primary ovarian tumors (52). Imaging findings in metastatic lesions are nonspecific, consisting of predominantly solid components or a mixture of cystic and solid areas (52). However, Krukenberg tumor demonstrates some distinctive findings, including bilateral complex masses with hypointense solid components (dense stromal reaction) and internal hyperintensity (mucin) on T1- and T2-weighted MR images, respectively (Fig 28) (53).

Key Imaging Features in Differential Diagnosis

The imaging appearance of ovarian tumors ranges from cystic to solid masses. Although ovarian tumors have similar clinical and radiologic findings, predominant or specific key features are present in each type of ovarian tumor.

1. Serous cystadenoma is a thin-walled, unilocular or multilocular tumor filled with serous fluid. This tumor is very common and may mimic a physiologic cyst or, occasionally, an atypical mature cystic teratoma that lacks the characteristic eccentric mural nodule.

2. Mucinous cystadenoma is less common, is almost always multilocular, and may be large. In many of these tumors, the MR imaging and CT appearance of the individual locules may vary as a result of differences in degree of hemorrhage or protein content.

3. Although there is considerable overlap in morphologic characteristics and corresponding imaging features that in many cases prevents definitive preoperative characterization as benign or malignant, features that are suggestive of malignant epithelial tumors include a thick, irregular wall; thick septa; papillary projections; and a large soft-tissue component with necrosis.

4. Ovarian tumors associated with endometrial hyperplasia or carcinoma include endometrioid carcinoma, granulosa cell tumor, and, occasionally, thecoma or fibrothecoma.

5. Solid ovarian tumors that have very low signal intensity on T2-weighted MR images include fibroma, Brenner tumor, and, occasionally, fibrothecoma.

6. Although rare, endometrioid carcinoma is the most common malignant neoplasm that arises from endometriosis, followed by clear cell carcinoma.

7. The presence of fat opacity or fat signal intensity in an ovarian lesion is highly specific for a teratoma. Mature cystic teratomas are predominantly cystic with dense calcifications, whereas immature teratomas are predominantly solid with small foci of lipid material and scattered calcifications.

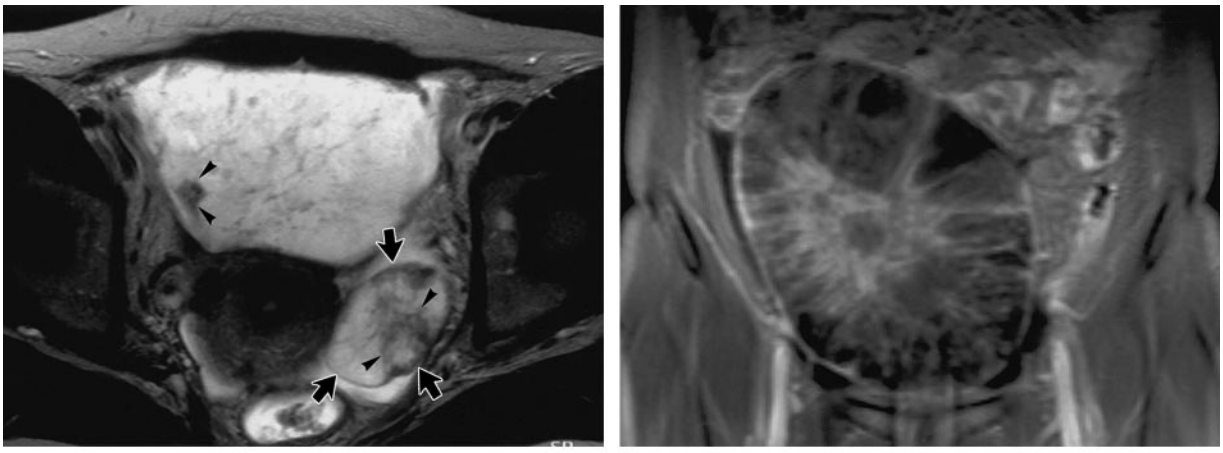

a. b.

Figure 28. Bilateral Krukenberg tumors from gastric carcinoma in a 38-year-old woman. **(a)** Axial turbo spin-echo T2-weighted MR image (5,200/132) shows bilateral cystic masses with hypointense solid portions (arrowheads). The left-sided mass (arrows) is much smaller than the right-sided mass. **(b)** Gadolinium-enhanced fat-suppressed FLASH T1-weighted MR image (147/4.8) shows the mass with marked enhancement of the septa and solid components.

8. Malignant germ cell tumors include dysgerminoma and endodermal sinus tumors, among others. These are large, predominantly solid masses that are more common in younger women (second and third decades of life). Dysgerminoma may demonstrate prominent fibrovascular septa. Serum tumor markers may be useful in making the diagnosis of malignant germ cell tumor.

9. Ovarian tumors with highly enhancing solid portions, although uncommon, include sclerosing stromal tumor, Sertoli-Leydig cell tumor, struma ovarii, and cystadenofibroma.

10. Ovarian tumors that are frequently associated with calcifications include serous epithelial tumor, fibrothecoma, mature or immature teratoma, and Brenner tumor.

11. When bilateral complex ovarian masses are seen, metastatic ovarian tumors and serous epithelial tumors of the ovary should be considered.

12. When an ovarian tumor demonstrates imaging findings that cannot be subsumed under one histologic type (especially in cases of ovarian teratoma), a collision tumor should be considered.

Conclusions

Ovarian tumors can be categorized as epithelial, germ cell, sex cord–stromal, and metastatic. Epithelial tumors are the most common type of ovarian tumor. They are primarily cystic, may be either unilocular or multilocular, and, if malignant, are associated with varying proportions of a solid component. Papillary projections are a distinctive feature of epithelial tumors. Profuse papillary projections are highly suggestive of low-malignant-potential or malignant epithelial tumors.

Mature cystic teratomas manifest as a diffusely or partially echogenic mass, with the echogenic area usually demonstrating sound attenuation at US owing to the presence of sebaceous material. At CT and MR imaging, ovarian teratomas (mature and immature) exhibit lipid material. Malignant germ cell tumors manifest as a large, complex pelvic mass that contains both solid and cystic components. Tumor markers are helpful in making this diagnosis.

The radiologic appearance of sex cord–stromal tumors varies from a small, solid mass to a large, multicystic mass. Granulosa cell tumors are usually large, multicystic masses with solid components. Fibrothecomas, sclerosing stromal tumors, and Sertoli-Leydig cell tumors are usually solid masses. Fibromas manifest as a homogeneous hypoechoic mass with posterior acoustic shadowing at US and have very low signal intensity on T2-weighted MR images. Sclerosing stromal tumors have a highly enhancing portion.

Certain radiologic findings predominate for each type of tumor. Knowledge of these key imaging features of ovarian tumors may allow a specific diagnosis or substantial narrowing of the differential diagnosis. Characterization of ovarian tumors can aid in surgical planning, whether exploration or laparoscopic excision, and may help distinguish benign from malignant tumors and thus avoid inappropriate management.

Acknowledgment: We thank Bonnie Hami, MA, Department of Radiology, University Hospitals Health System, Cleveland, Ohio, for editorial assistance in preparing the manuscript.

References

1. Koonings PP, Campbell K, Mishell DR Jr, Grimes DA. Relative frequency of primary ovarian neoplasms: a 10-year review. Obstet Gynecol 1989; 74:921–926.
2. Herrmann UI Jr, Locher GW, Goldhirsh A. Sonographic patterns of ovarian tumors: prediction of malignancy. Obstet Gynecol 1987; 69:777–781.
3. Parker WH, Berek JS. Laparoscopic management of the adnexal mass. Obstet Gynecol Clin North Am 1994; 21:79–92.
4. Russell P. Surface epithelial-stromal tumors of the ovary. In: Kurman RJ, ed. Blaustein's pathology of the female genital tract. 4th ed. New York, NY: Springer-Verlag, 1994; 705–782.
5. Richardson GS, Scully RE, Nikrui N, Nelson JH Jr. Common epithelial cancer of the ovary (2). N Engl J Med 1985; 312:474–483.
6. Kawamoto S, Urban BA, Fishman EK. CT of epithelial ovarian tumors. RadioGraphics 1999; 19: S85–S102.
7. Jeong YY, Outwater EK, Kang HK. Imaging evaluation of ovarian masses. RadioGraphics 2000; 20:1445–1470.
8. Ghossain MA, Buy JN, Ligneres C, et al. Epithelial tumors of the ovary: comparison of MR and CT findings. Radiology 1991; 181:863–870.
9. Pretorius ES, Outwater EK, Hunt JL, Siegelman ES. Magnetic resonance imaging of the ovary. Top Magn Reson Imaging 2001; 12:131–146.
10. Occhipinti KA. Computed tomography and magnetic resonance imaging of the ovary. In: Anderson JC, ed. Gynecologic imaging. London, England: Churchill Livingstone, 1999; 345–359.
11. Buy JN, Ghossain MA, Sciot C, et al. Epithelial tumors of the ovary: CT findings and correlation with US. Radiology 1991; 178:811–818.
12. Wagner BJ, Buck JL, Seidman JD, McCabe KM. Ovarian epithelial neoplasms: radiologic-pathologic correlation. RadioGraphics 1994; 14:1351–1374.
13. Kurtz AB, Tsimikas JV, Tempany CM, et al. Diagnosis and staging of ovarian cancer: comparative values of Doppler and conventional US, CT, and MR imaging correlated with surgery and histopathologic analysis—report of the Radiology Diagnostic Oncology Group. Radiology 1999; 212:19–27.
14. Barakat RR. Borderline tumors of the ovary. Obstet Gynecol Clin North Am 1994; 21:93–105.
15. Krigman H, Bentley R, Robboy SJ. Pathology of epithelial ovarian tumors. Clin Obstet Gynecol 1994; 37:475–491.
16. Outwater EK, Huang AB, Dunton CJ, Talerman A, Capuzzi DM. Papillary projections in ovarian neoplasms: appearance on MRI. J Magn Reson Imaging 1997; 7:689–695.
17. Outwater EK, Dunton CJ. Imaging of the ovary and adnexa: clinical issues and applications of MR imaging. Radiology 1995; 194:1–18.
18. Tanaka YO, Yoshizako T, Nishida M, Yamaguchi M, Sugimura K, Itai Y. Ovarian carcinoma in patients with endometriosis: MR imaging findings. AJR Am J Roentgenol 2000; 175:1423–1430.
19. Woodward PJ, Sohaey R, Mezzetti TP Jr. Endometriosis: radiologic-pathologic correlation. RadioGraphics 2001; 21:193–216.
20. Tornos C, Silva EG. Pathology of epithelial ovarian cancer. Obstet Gynecol Clin North Am 1994; 21:63–77.
21. Matsuoka Y, Ohtomo K, Araki T, Kojima K, Yoshikawa W, Fuwa S. MR imaging of clear cell carcinoma of the ovary. Eur Radiol 2001; 11:946–951.
22. Moon WJ, Koh BH, Kim SK, et al. Brenner tumor of the ovary: CT and MR findings. J Comput Assist Tomogr 2000; 24:72–76.
23. Outwater EK, Siegelman ES, Kim B, Chiowanich P, Blasbalg R, Kilger A. Ovarian Brenner tumors: MR imaging characteristics. Magn Reson Imaging 1998; 16:1147–1153.
24. Brammer HM III, Buck JL, Hayes WS, Sheth S, Tavassoli FA. Malignant germ cell tumors of the ovary: radiologic-pathologic correlation. RadioGraphics 1990; 10:715–724.
25. Comerci JT Jr, Licciardi F, Bergh PA, Gregori C, Breen JL. Mature cystic teratoma: a clinicopathologic evaluation of 517 cases and review of the literature. Obstet Gynecol 1994; 84:22–28.
26. Outwater EK, Siegelman ES, Hunt JL. Ovarian teratomas: tumor types and imaging characteristics. RadioGraphics 2001; 21:475–490.
27. Quinn SF, Erickson S, Black WC. Cystic ovarian teratomas: the sonographic appearance of the dermoid plug. Radiology 1985; 155:477–478.
28. Patel MD, Feldstein VA, Lipson SD, Chen DC, Filly RA. Cystic teratomas of the ovary: diagnostic value of sonography. AJR Am J Roentgenol 1998; 171:1061–1065.

29. Buy JN, Ghossain MA, Moss AA, et al. Cystic teratoma of the ovary: CT detection. Radiology 1989; 171:697–701.
30. Guinet C, Ghossain MA, Buy JN, et al. Mature cystic teratomas of the ovary: CT and MR findings. Eur J Radiol 1995; 20:137–143.
31. Kido A, Togashi K, Konishi I, et al. Dermoid cysts of the ovary with malignant transformation: MR appearance. AJR Am J Roentgenol 1999; 172: 445–449.
32. Kim SH, Kang SB. Ovarian dysgerminoma: color Doppler ultrasonographic findings and comparison with CT and MR imaging findings. J Ultrasound Med 1995; 14:843–848.
33. Tanaka YO, Kurosaki Y, Nishida M, et al. Ovarian dysgerminoma: MR and CT appearance. J Comput Assist Tomogr 1994; 18:443–448.
34. Levitin A, Haller KD, Cohen HL, Zinn DL, O'Connor MT. Endodermal sinus tumor of the ovary: imaging evaluation. AJR Am J Roentgenol 1996; 167:791–793.
35. Yamaoka T, Togashi K, Koyama T, et al. Yolk sac tumor of the ovary: radiologic-pathologic correlation in four cases. J Comput Assist Tomogr 2000; 24:605–609.
36. Outwater EK, Wagner BJ, Mannion C, McLarney JK, Kim B. Sex cord–stromal and steroid cell tumors of the ovary. RadioGraphics 1998; 18:1523–1546.
37. Ko SF, Wan YL, Ng SH, et al. Adult ovarian granulosa cell tumors: spectrum of sonographic and CT findings with pathologic correlation. AJR Am J Roentgenol 1999; 172:1227–1233.
38. Morikawa K, Hatabu H, Togashi K, Kataoka ML, Mori T, Konishi J. Granulosa cell tumor of the ovary: MR findings. J Comput Assist Tomogr 1997; 21:1001–1004.
39. Fink D, Kubik-Huch RA, Wildermuth S. Juvenile granulosa cell tumor. Abdom Imaging 2001; 26: 550–552.
40. Troiano RN, Lazzarini KM, Scoutt LM, Lange RC, Flynn SD, McCarthy S. Fibroma and fibrothecoma of the ovary: MR imaging findings. Radiology 1997; 204:795–798.
41. Athey PA, Malone RS. Sonography of ovarian fibromas/thecomas. J Ultrasound Med 1987; 6: 431–436.
42. Bazot M, Ghossain MA, Buy JN, et al. Fibrothecomas of the ovary: CT and US findings. J Comput Assist Tomogr 1993; 17:754–759.
43. Kim SH, Sim JS, Seong CK. Interface vessels on color/power Doppler US and MRI: a clue to differentiate subserosal uterine myomas from extrauterine tumors. J Comput Assist Tomogr 2001; 25: 36–42.
44. Torashima M, Yamashita Y, Matsuno Y, et al. The value of detection of flow voids between the uterus and the leiomyoma with MRI. J Magn Reson Imaging 1998; 8:427–431.
45. Matsubayashi R, Matsuo Y, Doi J, Kudo S, Matsuguchi K, Sugimori H. Sclerosing stromal tumor of the ovary: radiologic findings. Eur Radiol 1999; 9:1335–1338.
46. Joja I, Okuno K, Tsunoda M, et al. Sclerosing stromal tumor of the ovary: US, MR, and dynamic MR findings. J Comput Assist Tomogr 2001; 25: 201–206.
47. Ihara N, Togashi K, Todo G, et al. Sclerosing stromal tumor of the ovary: MRI. J Comput Assist Tomogr 1999; 23:555–557.
48. Outwater EK, Marchetto B, Wagner BJ. Virilizing tumors of the ovary: imaging features. Ultrasound Obstet Gynecol 2000; 15:365–371.
49. Kim SH, Kim YJ, Park BK, Cho JY, Kim BH, Byun JY. Collision tumors of the ovary associated with teratoma: clues to the correct preoperative diagnosis. J Comput Assist Tomogr 1999; 23: 929–933.
50. Dgani R, Rozenman D, Lifschitz-Mercer B. Granulosa cell tumor arising in an ovary with mature cystic teratoma. Int J Gynaecol Obstet 1993; 41:287–289.
51. Bichel P. Simultaneous occurrence of a granulosa cell tumour and a serous papillary cystadenocarcinoma in the same ovary: a case report. Acta Pathol Microbiol Immunol Scand [A] 1985; 93: 175–181.
52. Brown DL, Zou KH, Tempany CM, et al. Primary versus secondary ovarian malignancy: imaging findings of adnexal masses in the Radiology Diagnostic Oncology Group Study. Radiology 2001; 219:213–218.
53. Ha HK, Baek SY, Kim SH, Kim HH, Chung EC, Yeon KM. Krukenberg's tumor of the ovary: MR imaging features. AJR Am J Roentgenol 1995; 164:1435–1439.

This article meets the criteria for 1.0 credit hour in category 1 of the AMA Physician's Recognition Award. To obtain credit, see accompanying test at http://www.rsna.org/education/rg_cme.html.